




One-dimensional harmonic chain model of vibration-mode matching in solid-liquid interfacial thermal transport

Hiroki Matsubara ^{*}, Donatas Surblys , and Taku Ohara 

Institute of Fluid Science, Tohoku University, 2-1-1 Katahira, Aoba-ku, Sendai 980-8577, Japan



(Received 7 September 2022; accepted 6 January 2023; published 1 February 2023)

Understanding the atomistic mechanism of interfacial thermal transport at solid-liquid interfaces is a key challenge in thermal management at the nanoscale. A recent molecular-dynamics study demonstrated that interfacial thermal resistance (ITR) at the interface between a solid and a surfactant solution can be minimized by adjusting the molecular mass of the surfactant. In the present study, we explain the mechanism of this ITR minimization in view of vibration-mode matching using a one-dimensional (1D) harmonic chain model of a solid-liquid interface having an interfacial adsorption layer of surfactant molecules. The equation of motion for the 1D chain is described by a classical Langevin equation and is analytically solved by the nonequilibrium Green's function (NEGF) method. The resultant ITR is expressed in a form of vibrational matching, and its relationship to the overlap of the vibrational density of states is also discussed. The analysis leads to a conclusion that the damping coefficient η in the Langevin equation should be a finite and sufficiently large value to represent the rapid damping of vibration modes at solid-liquid interfaces. This conclusion provides a clue to seamlessly extend the conventional NEGF-phonon transmission picture of solid-solid interfacial thermal transport, which assumes η to be infinitesimal, to solid-liquid interfaces.

DOI: [10.1103/PhysRevE.107.024103](https://doi.org/10.1103/PhysRevE.107.024103)

I. INTRODUCTION

Understanding the atomistic mechanism of interfacial thermal transport at solid-liquid interfaces is a key challenge in thermal management at the nanoscale. Relevant examples of such interfaces include the interfaces between filler particles and base liquids in nanofluids [1] and those between heat-generating/dissipating components and thermal interface materials (TIMs) [2]. Current understanding of solid-liquid interfacial thermal transport remains qualitative, relying largely on empirical correlations between interfacial thermal transport and solid-liquid affinity or interfacial structures, which have been found by experiments [3,4] and molecular simulations [5–7].

In contrast, for interfacial thermal transport between solid insulators, sophisticated atomistic theories have been developed based on the phonon picture [8]. In the Landauer approach [9], the transmission function α_j dictates the ratio of transmitted energy when a phonon mode j is incident on an interface of two materials. Interfacial thermal conductance (ITC) is expressed as the accumulation of such phonon energy transmission. Therefore, ITC or interfacial thermal resistance (ITR), defined as the reciprocal of ITC, can be calculated if α_j is known for all phonon modes. The transmission function

can be evaluated in various ways, including simple approximations such as the acoustic mismatch model (AMM) and the diffuse mismatch model (DMM) [10,11], rigorous theories such as the nonequilibrium Green's function (NEGF) theory [12,13], and molecular simulations such as the phonon wavepacket dynamics [14,15]. In addition, when one investigates interfacial thermal transport using molecular-dynamics (MD) simulations, it is a common practice to calculate the overlap of the vibrational density of states (VDOS) on both sides of an interface [16]. The VDOS overlap may be viewed as a rough estimator of the average phonon transmission.

To explore a way to extend the phonon transmission picture to solid-liquid interfaces, the present study focuses on surfactants. Surfactants are used to reduce solid-liquid ITR [1,17,18], but from a theoretical viewpoint they can also be considered a means of systematically altering the vibrational characteristics at interfaces. Based on this idea, we recently conducted MD simulations for model interfaces between solid crystals and surfactant solutions where the solid atom, surfactant molecule, and solvent molecule are all represented by a single atom [19]. The MD simulations demonstrated that ITR of the model interface can be minimized by adjusting the mass of the surfactant molecule. The minimum ITR is likely due to the best matching in vibration modes between the solid, surfactant, and solvent particles. Although this vibrational matching is likely an important clue towards the phonon transmission model of solid-liquid interfacial thermal transport, its mechanism remained to be elucidated. In particular, the optimal surfactant mass was not the one that maximizes the VDOS overlap between the relevant particles.

In the present study, we attempt to clarify the detailed mechanism of the vibration-mode matching by further

^{*}Corresponding author: matsubara@microheat.ifs.tohoku.ac.jp

Published by the American Physical Society under the terms of the Creative Commons Attribution 4.0 International license. Further distribution of this work must maintain attribution to the author(s) and the published article's title, journal citation, and DOI.

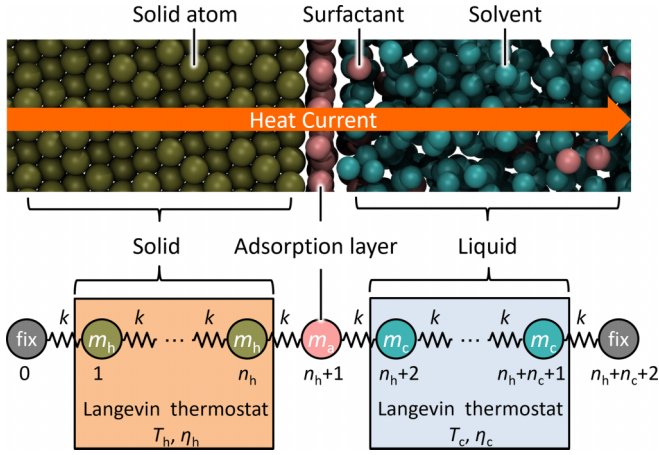


FIG. 1. Interface between the solid and surfactant solution in the reference system of Ref. [19] (top), and its one-dimensional harmonic chain (bottom) model, consisting of n_h h-particles, one a-particle, and n_c c-particles.

simplifying the above-mentioned model interface of a solid and a surfactant solution as a one-dimensional (1D) harmonic chain. The equation of motion for the chain particles is described by a classical Langevin equation, and it can be solved analytically. From the analytic solution, we derive an explicit relation between the ITR minimization and vibration-mode matching.

We use the NEGF approach to analytically solve the Langevin equation. The standard NEGF formulation for heat conduction [12,13,20] basically solves the Schrödinger equation of phonons in a material in contact with heat reservoirs, where a positive infinitesimal parameter η is introduced. This parameter is known to represent the removal of energy from the reservoirs [21], but the meaning of its value is somewhat confusing. Independent of the Schrödinger formulation, Dhar *et al.* have developed another NEGF formulation based on a quantum Langevin equation [22,23]. While the two formulations are mathematically equivalent, in the Langevin form η is more clearly interpreted as the damping coefficient in the viscous drag term. Here, we use the Langevin formulation, but we solve the classical Langevin equation, rather than the quantum one. This treatment enables a stringent comparison between the NEGF analysis and MD simulations, since the same Langevin equation can be numerically solved by MD simulations. Because such a full classical treatment of the NEGF theory is not well documented, we will give a detailed theoretical formulation in Sec. II B, together with a supplementary explanation in the Appendix.

II. METHOD AND THEORY

A. One-dimensional harmonic chain model of solid-liquid interfaces

Independent of whether surfactants are added or not, a solid-liquid interface has a liquid adsorption layer of a few molecules thick on the solid surface, which has physical properties different from those in the bulk liquid region. Considering this, we divide a solid-liquid interface into three regions as illustrated in Fig. 1: the solid region, liquid ad-

sorption layer, and bulk liquid region, and these regions are modeled by a 1D harmonic chain with n_h h-particles, n_a a-particles, and n_c c-particles, respectively. The chain is terminated by one fixed particle on each side. In the present study, we mainly assume $n_a = 1$, although many of the NEGF expressions will be derived for $n_a \geq 1$. The whole chain is indexed in order from 0 to $n_h + n_a + n_c + 1$, and two adjacent particles are connected by a harmonic potential. The h-particles are in contact with a hot Langevin thermostat of temperature T_h and the damping coefficient η_h , while the c-particles are in contact with a cold Langevin thermostat of temperature T_c and the damping coefficient η_c , in order to impose a heat current from the h-particles to the c-particles. We refer to the h- and c-particles collectively as reservoir particles. The total number of mobile particles is $n_{\text{tot}} = n_h + n_a + n_c$ with indices $1 \leq j \leq n_{\text{tot}}$. The equation of motion for the j th particle is described by the following Langevin equation in terms of mass-scaled variables:

$$\ddot{u}_j(t) = -K_{j,j-1}u_{j-1}(t) - K_{jj}u_j(t) - K_{j,j+1}u_{j+1}(t) - \eta_j \dot{u}_j(t) + s_j(t), \quad (1)$$

where $u_j(t) = m_j^{1/2}[x_j(t) - \bar{x}_j]$ is the mass-scaled displacement [24] at time t , m_j is the particle mass, $x_j(t)$ is the particle position, \bar{x}_j is the equilibrium position, and an overdot denotes a time derivative. If j is the index of the fixed particles, u_j is always set to 0. The force constant matrix K_{jl} is defined as

$$K_{jl} = \begin{cases} -k_{jl}/\sqrt{m_j m_l} & \text{if } l \neq j, \\ (k_{j-1,j} + k_{j,j+1})/m_j & \text{if } l = j, \end{cases} \quad (2)$$

where k_{jl} is the spring constant of the harmonic potential between j and l . The last two terms on the right-hand side of Eq. (1) are considered only for reservoir particles, where η_j is the damping coefficient and $s_j(t)$ is the random force. These variables are assumed to obey the fluctuation-dissipation relation:

$$\langle s_j(t) s_l(t') \rangle = 2\eta_j k_B T_j \delta(t - t') \delta_{jl}, \quad (3)$$

where $\langle \dots \rangle$ is the ensemble average, k_B is the Boltzmann constant, $\delta(t-t')$ is the Dirac delta function, and δ_{jl} is the Kronecker delta. For h-particles, $T_j = T_h$ and $\eta_j = \eta_h$ while for c-particles, $T_j = T_c$ and $\eta_j = \eta_c$.

In the present study, the parameters in the 1D model were adjusted with reference to the MD system of the solid-surfactant solution interface for the case of low affinity in Ref. [19], and we call it the reference system hereafter. In the reference system, ITR was calculated as a function of the mass of surfactant molecule, m_{srf} , while the properties of the solid and solvent particles were fixed. For surfactant concentration in the range 5–50 mol %, the ITR was minimized at $m_{\text{srf}}/m_{\text{solv}} = 0.2\text{--}0.3$, where m_{solv} is the mass of the solvent molecule. Since the adsorption layer and bulk liquid region in the reference system mostly consisted of surfactant and solvent molecules, respectively, we consider that a-particles represent the surfactant molecules and c-particles represent the solvent molecules. The values of spring constant and particle mass were set such that h-, a-, and c-particles approximately reproduce the PMF frequency in the solid, first adsorption layer, and bulk liquid region of the reference

TABLE I. Properties relevant to the harmonic frequencies of h-, a-, and c-particles. The second column is the particle mass in the 1D chain model. The other columns are the properties of the reference system of Ref. [19]: f_{XY}^{PMF} is the PMF frequency, k_{XY}^{PMF} is the corresponding spring constant, and the fifth and sixth columns are the region and particle pair for which the PMF was calculated, respectively. The mass and f_{XY}^{PMF} of the a-particle are variable parameters.

	1D chain		Reference system		
	mass (u)	f_{XY}^{PMF} (THz)	k_{XY}^{PMF} (J/m ²)	region	X-Y pair
h-particle	1.381	5.36	183.7	bulk solid	solid atom pair
a-particle			1.2	First adsorption layer	surfactant pair
c-particle	39.95	1.0	1.3	bulk liquid	solvent pair

system, respectively. Here, the PMF stands for the potential of mean force, and the PMF frequency between two particles X and Y is defined as

$$f_{XY}^{\text{PMF}} = \frac{1}{2\pi} \sqrt{\frac{k_{XY}^{\text{PMF}}}{M_{XY}}}, \quad (4)$$

where $M_{XY} = m_X m_Y / (m_X + m_Y)$ is the reduced mass, and k_{XY}^{PMF} is the spring constant of the PMF between X and Y [19]. Since the PMF is regarded as an effective pair potential between the X-Y pair under the existence of surrounding particles, the PMF frequency is expected to serve as a representative frequency in each region. In liquids, the lifetime of this vibration may be considerably short. However, we found in Ref. [19] that the matching in the PMF frequency leads to the maximum thermal conductance between the first and second adsorption liquid layers on a solid surface. Thus, the PMF frequency likely qualifies as a characteristic frequency in liquids. The values of f_{XY}^{PMF} and k_{XY}^{PMF} are listed in Table I, and hereafter these quantities calculated for the solid region, first adsorption layer, and liquid region are distinguished by the subscripts ‘‘solid,’’ ‘‘adlayer,’’ and ‘‘liquid,’’ respectively. The spring constant of the PMF for the liquid region was calculated as $k_{\text{liquid}}^{\text{PMF}} = 1.3 \text{ J/m}^2$. In the 1D model, the spring constant k was set equal to this value for all interacting pairs. Therefore, the difference in vibrational frequency was achieved by particle mass: i.e., the masses of h-, a-, and c-particles were set to $m_h = m_{\text{solv}} (f_{\text{liquid}}^{\text{PMF}} / f_{\text{solid}}^{\text{PMF}})^2$, $m_a = m_{\text{solv}} (f_{\text{liquid}}^{\text{PMF}} / f_{\text{adlayer}}^{\text{PMF}})^2$, and $m_c = m_{\text{solv}}$, respectively, where $m_{\text{solv}} = 39.95 \text{ u}$ is the mass of the solvent particle (argon atom) in the reference system. The relation $m_a = m_{\text{solv}} (f_{\text{liquid}}^{\text{PMF}} / f_{\text{adlayer}}^{\text{PMF}})^2$ can be rewritten as $m_a = m_{\text{srf}} k_{\text{liquid}}^{\text{PMF}} / k_{\text{adlayer}}^{\text{PMF}}$. If we ignore the small difference between $k_{\text{liquid}}^{\text{PMF}}$ and $k_{\text{adlayer}}^{\text{PMF}}$ (8% according to Table I), then $m_a = m_{\text{srf}}$ holds. Thus, we can reasonably consider that the 1D chain models the reference system in which the surfactant mass is equal to m_a .

B. Nonequilibrium Green's function method

In this subsection, we consider the solution of the Langevin equation (1) using the NEGF method, assuming that the number of a-particles, n_a , is an arbitrary natural number. The solution is carried out in the frequency domain. We define the Fourier transforms of a variable X between the time and frequency domain by

$$X(\omega) = \frac{1}{2\pi} \int X(t) e^{i\omega t} dt \quad \text{and} \quad X(t) = \int X(\omega) e^{-i\omega t} d\omega, \quad (5)$$

where i is the imaginary unit, t is time, and ω is angular frequency. Fourier transforming Eq. (1) into the frequency domain and grouping variables into matrices and vectors by different particle types, we obtain the following matrix equation:

$$\begin{pmatrix} \mathbf{g}_h^{-1}(\omega) & -\mathbf{K}_{\text{ha}} & \\ -\mathbf{K}_{\text{ha}}^+ & \omega^2 \mathbf{I}_a - \mathbf{K}_a & -\mathbf{K}_{\text{ca}}^+ \\ & -\mathbf{K}_{\text{ca}} & \mathbf{g}_c^{-1}(\omega) \end{pmatrix} \begin{pmatrix} \mathbf{u}_h(\omega) \\ \mathbf{u}_a(\omega) \\ \mathbf{u}_c(\omega) \end{pmatrix} = \begin{pmatrix} -\mathbf{s}_h(\omega) \\ \mathbf{0} \\ -\mathbf{s}_c(\omega) \end{pmatrix}. \quad (6)$$

This matrix form, as well as the following derivation, is based on Datta [21], although other matrix representations are also possible. Let us first summarize some notations. The variables of reservoir particles are denoted by μ , which means either h or c. Matrices and vectors are shown in boldface, and \mathbf{I}_a and \mathbf{I}_μ are the $n_a \times n_a$ and $n_\mu \times n_\mu$ unit matrices, respectively. We use $o_h = 1$, $o_a = n_h + 1$, and $o_c = n_h + n_a + 1$ as the index offsets of the h-, a-, and c-particles, respectively. The transpose, complex conjugate, and Hermitian conjugate of \mathbf{X} are denoted by \mathbf{X}^T , \mathbf{X}^* , and $\mathbf{X}^+ = (\mathbf{X}^T)^*$, respectively. The trace of a matrix \mathbf{X} is designated by $\text{Tr}[\mathbf{X}]$, and we note that matrices \mathbf{X} and \mathbf{Y} commute inside the trace as $\text{Tr}[\mathbf{X}\mathbf{Y}] = \text{Tr}[\mathbf{Y}\mathbf{X}]$. When \mathbf{X} and \mathbf{Y} are a column vector, $\mathbf{X}\mathbf{Y}^T \equiv \mathbf{X} \otimes \mathbf{Y}$ is a matrix defined by the tensor product, whereas $\mathbf{Y}^T \mathbf{X} \equiv \mathbf{Y} \cdot \mathbf{X} = \text{Tr}[\mathbf{X}\mathbf{Y}^T]$ means a dot product. The components of matrices in Eq. (6) are as follows:

Displacement vectors:

$$\begin{aligned} \mathbf{u}_a(\omega) &= (u_{o_a}(\omega), \dots, u_{o_a+n_a-1}(\omega))^T \quad \text{and} \\ \mathbf{u}_\mu(\omega) &= (u_{o_\mu}(\omega), \dots, u_{o_\mu+n_\mu-1}(\omega))^T. \end{aligned} \quad (7)$$

Random force vector:

$$\mathbf{s}_\mu(\omega) = (s_{o_\mu}(\omega), \dots, s_{o_\mu+n_\mu-1}(\omega))^T. \quad (8)$$

Damping coefficient matrix:

$$\boldsymbol{\eta}_\mu = \boldsymbol{\eta}_\mu \mathbf{I}_\mu. \quad (9)$$

Coupling force constant matrix ($n_\mu \times n_a$ matrix):

$$\begin{aligned} \mathbf{K}_{\text{ha}} &= \begin{pmatrix} 0 & \cdots & 0 \\ \vdots & \ddots & \vdots \\ K_{o_a, o_a-1} & \cdots & 0 \end{pmatrix} \quad \text{and} \\ \mathbf{K}_{\text{ca}} &= \begin{pmatrix} 0 & \cdots & K_{o_c-1, o_c} \\ \vdots & \ddots & \vdots \\ 0 & \cdots & 0 \end{pmatrix}. \end{aligned} \quad (10)$$

Force constant matrix of a-particle ($n_a \times n_a$ tridiagonal matrix):

$$\mathbf{K}_a = \begin{pmatrix} K_{o_a, o_a} & K_{o_a, o_a+1} & & \\ K_{o_a+1, o_a} & \ddots & \ddots & \\ & \ddots & \ddots & \\ & & & K_{o_a+n_a-1, o_a+n_a-1} \end{pmatrix}. \quad (11)$$

Force constant matrix of μ -particle ($n_\mu \times n_\mu$ tridiagonal matrix):

$$\mathbf{K}_\mu = \begin{pmatrix} K_{o_\mu, o_\mu} & K_{o_\mu, o_\mu+1} & & \\ K_{o_\mu+1, o_\mu} & \ddots & \ddots & \\ & \ddots & \ddots & \\ & & & K_{o_\mu+n_\mu-1, o_\mu+n_\mu-1} \end{pmatrix}. \quad (12)$$

Green's function for the μ -particle ($n_\mu \times n_\mu$ symmetric matrix):

$$\mathbf{g}_\mu(\omega) = \frac{1}{\omega^2 \mathbf{I}_\mu - \mathbf{K}_\mu + i\omega \boldsymbol{\eta}_\mu}. \quad (13)$$

Damping coefficient matrix:

$$\boldsymbol{\eta}_\mu = \eta_\mu \mathbf{I}_\mu. \quad (14)$$

Let us first consider the uncoupled state where the μ -particle system is not connected to the a-particle system by setting the coupling matrices $\mathbf{K}_{\mu a}$ and $\mathbf{K}_{\mu a}^+$ in Eq. (6) all to zero. The displacement vector of μ -particles in this case is readily obtained from the first and third rows of Eq. (6) as

$$\mathbf{u}_\mu^0(\omega) = -\mathbf{g}_\mu(\omega) \mathbf{s}_\mu(\omega). \quad (15)$$

Suppose that the displacement changed by $\Delta \mathbf{u}_\mu$ when the coupling matrices are turned back on. Then, we can write $\mathbf{u}_\mu(\omega) = \mathbf{u}_\mu^0(\omega) + \Delta \mathbf{u}_\mu(\omega)$. Inserting this into the first and third rows of Eq. (6) and applying Eq. (15), we find $\Delta \mathbf{u}_\mu(\omega) = \mathbf{g}_\mu(\omega) \mathbf{K}_{\mu a} \mathbf{u}_a(\omega)$, and therefore

$$\mathbf{u}_\mu(\omega) = \mathbf{u}_\mu^0(\omega) + \mathbf{g}_\mu(\omega) \mathbf{K}_{\mu a} \mathbf{u}_a(\omega). \quad (16)$$

Using Eq. (16) in the second row of Eq. (6), \mathbf{u}_a is found to be

$$\mathbf{u}_a(\omega) = \mathbf{g}_a(\omega) \mathbf{K}_{ha}^+ \mathbf{u}_h^0(\omega) + \mathbf{g}_a(\omega) \mathbf{K}_{ca}^+ \mathbf{u}_c^0(\omega), \quad (17)$$

where

$$\mathbf{g}_a(\omega) = \frac{1}{\omega^2 \mathbf{I}_a - \mathbf{K}_a - \boldsymbol{\Sigma}_h(\omega) - \boldsymbol{\Sigma}_c(\omega)} \quad (18)$$

is the Green's function of an a-particle, and

$$\boldsymbol{\Sigma}_\mu(\omega) = \mathbf{K}_{\mu a}^+ \mathbf{g}_\mu(\omega) \mathbf{K}_{\mu a} \quad (19)$$

is the self-energy. The imaginary part of $\boldsymbol{\Sigma}_\mu$ is denoted by a real symmetric matrix $\boldsymbol{\Gamma}_\mu$ as

$$\boldsymbol{\Gamma}_\mu(\omega) = -2\text{Im}[\boldsymbol{\Sigma}_\mu(\omega)] = i[\boldsymbol{\Sigma}_\mu(\omega) - \boldsymbol{\Sigma}_\mu^+(\omega)]. \quad (20)$$

The role of $\boldsymbol{\Gamma}_\mu$ in \mathbf{g}_a is similar to that of the damping coefficient matrix $\boldsymbol{\eta}_\mu$ in \mathbf{g}_μ .

The displacement vectors in Eqs. (16) and (17) constitute the solution of Eq. (6), but the solution contains the random force $\mathbf{s}_\mu(\omega)$, which is not an analytic function. As has been demonstrated by Dhar *et al.* [22,23], the analytic expression

for a physical quantity is obtained by eliminating $\mathbf{s}_\mu(\omega)$ from \mathbf{u}_μ and \mathbf{u}_a using the fluctuation-dissipation relation in the frequency domain:

$$\langle \mathbf{s}_\mu(\omega) \mathbf{s}_\mu^+(\omega') \rangle = \frac{\eta_\mu k_B T_\mu}{\pi} \delta(\omega - \omega') \delta_{\mu\mu'}, \quad (21)$$

which is the Fourier transform of Eq. (3) with respect to both t and t' . For example, the mass-weighted velocity autocorrelation function (VACF) of μ -particles at the uncoupled state becomes

$$\begin{aligned} D_\mu^0(t, t') &= \sum_{j=o_\mu}^{o_\mu+n_\mu} m_j \langle \dot{x}_j(t) \dot{x}_j(t') \rangle \\ &= \text{Tr}(\dot{\mathbf{u}}_\mu^0(t) \dot{\mathbf{u}}_\mu^{0+}(t')) \\ &= \text{Tr} \iint \omega' \mathbf{g}_\mu(\omega) \langle \mathbf{s}_\mu(\omega) \mathbf{s}_\mu^+(\omega') \rangle \mathbf{g}_\mu^+(\omega') \\ &\quad \times e^{-i\omega t + i\omega' t'} d\omega d\omega' \\ &= \int \text{Tr} \left[\omega^2 \mathbf{g}_\mu(\omega) \frac{\eta_\mu k_B T_\mu}{\pi} \mathbf{g}_\mu^+(\omega) \right] e^{-i\omega(t-t')} d\omega, \end{aligned} \quad (22)$$

where \mathbf{u}_μ^0 is given in Eq. (15), and Eq. (21) is applied at the final equality. This equation shows that the VACF depends only on the time difference $t-t'$ as it should be in a steady state, and the Fourier transform of $D_\mu^0(t-t')$ is defined as the VDOS:

$$D_\mu^0(\omega) = \text{Tr}[\mathbf{D}_\mu^0(\omega)] \equiv \text{Tr}[\mathbf{g}_\mu(\omega) \boldsymbol{\eta}_\mu \mathbf{g}_\mu^+(\omega) \omega^2 k_B T_\mu / \pi]. \quad (23)$$

The VDOS expressions at the coupled state can be similarly derived using the relations Eqs. (A1)–(A9) in the Appendix, and the final expressions are as follows. The VACF of a-particles is given by $D_a(t, t') = \text{Tr}(\dot{\mathbf{u}}_a(t) \dot{\mathbf{u}}_a^+(t'))$, and the corresponding VDOS is

$$D_a(\omega) = \sum_{\mu=h, c} \frac{k_B T_\mu}{2\pi} \omega \text{Tr}[\mathbf{g}_a(\omega) \boldsymbol{\Gamma}_\mu(\omega) \mathbf{g}_a^+(\omega)]. \quad (24)$$

The VACF of μ -particles is written as $D_\mu(t, t') = \text{Tr}(\dot{\mathbf{u}}_\mu(t) \dot{\mathbf{u}}_\mu^+(t'))$, and the corresponding VDOS is

$$D_\mu(\omega) = D_\mu^0(\omega) + 2\text{Re}[D_\mu^1(\omega)] + D_a(\omega) \mathbf{K}_{\mu a}^+ \mathbf{g}_\mu^+(\omega) \mathbf{g}_\mu(\omega) \mathbf{K}_{\mu a}, \quad (25)$$

where $D_\mu^1(\omega) = \text{Tr}[\mathbf{D}_\mu^0(\omega) \mathbf{g}_\mu(\omega) \mathbf{K}_{\mu a} \mathbf{g}_a(\omega) \mathbf{K}_{\mu a}^+]$.

Next, we derive the expression of heat current. The average rate of energy transfer per unit time from the j th to l th particle via a pair interaction is given by $J_{jl} = -\langle \dot{u}_j f_{jl} / 2 \rangle + \langle \dot{u}_l f_{lj} / 2 \rangle$ [25], where f_{jl} is the force on the j th particle due to the pair interaction with the l th particle. In the present case, collecting the terms proportional to k_{jl} in Eq. (1), we find $f_{jl} = -K_{jl} u_l + K'_{jl} u_j$, where $K'_{jl} = k_{jl} / m_j$, and $l = j-1$ or $j+1$. However, the second term $K'_{jl} u_j$ does not contribute to J_{jl} . This is because $\langle \dot{u}_j(t) K'_{jl} u_j(t) \rangle$ is the total time derivative of $K'_{jl} (u_j^2(t)) / 2$, which is time-independent at a steady state. Taking this into account, the average heat current from the h-reservoir to the a-particle system, J_{ha} , can be obtained by

summing up J_{jl} for j over h-particles and l over a-particles as

$$\begin{aligned} J_{\text{ha}}(t) &= \frac{1}{2} \langle \dot{\mathbf{u}}_{\text{h}}^+(t) \mathbf{K}_{\text{ha}} \mathbf{u}_{\text{a}}(t) - \dot{\mathbf{u}}_{\text{a}}^+(t) \mathbf{K}_{\text{ha}}^+ \mathbf{u}_{\text{h}}(t) \rangle \\ &= \iint J_{\text{ha}}(\omega, \omega') e^{-i(\omega-\omega')t} d\omega' d\omega, \end{aligned} \quad (26)$$

where $J_{\text{ha}}(\omega, \omega') = i\omega' \langle \mathbf{u}_{\text{h}}^+(\omega') \mathbf{K}_{\text{ha}} \mathbf{u}_{\text{a}}(\omega) - \mathbf{u}_{\text{a}}^+(\omega') \mathbf{K}_{\text{ha}}^+ \mathbf{u}_{\text{h}}(\omega) \rangle / 2$ is the spectral heat current. As described in the Appendix, inserting Eqs. (16) and (17) into $J_{\text{ha}}(\omega', \omega)$ and applying Eq. (21), one can finally find that Eq. (26) is independent of time t and is written in the following form:

$$J_{\text{ha}} = \frac{k_{\text{B}}(T_{\text{h}} - T_{\text{c}})}{2\pi} \int_0^\infty \alpha(\omega) d\omega, \quad (27)$$

where

$$\begin{aligned} \alpha(\omega) &= \text{Tr}[\Gamma_{\text{h}}(\omega) \mathbf{g}_{\text{a}}^+(\omega) \Gamma_{\text{c}}(\omega) \mathbf{g}_{\text{a}}(\omega)] \\ &= \text{Tr}[\Gamma_{\text{c}}(\omega) \mathbf{g}_{\text{a}}^+(\omega) \Gamma_{\text{h}}(\omega) \mathbf{g}_{\text{a}}(\omega)] \end{aligned} \quad (28)$$

is the transmission function and satisfies $0 \leq \alpha(\omega) \leq 1$. The transmission function in the form of Eq. (28) is called the Calori formula [9], and the second equality is proven in the Appendix [Eq. (A5)]. From Eq. (27), ITC between the h- and c-reservoirs becomes

$$G = \frac{k_{\text{B}}}{2\pi} \int_0^\infty \alpha(\omega) d\omega, \quad (29)$$

and the corresponding ITR is given by $R = 1/G$.

C. Simulation

To confirm the NEGF expressions derived in Sec. II B, the Langevin equation (1) was also solved by MD simulations using the large-scale atomic/molecular massively parallel simulator (LAMMPS) software package [26,27]. The MD simulations were carried out for three chain lengths $n_{\text{tot}} = n_{\text{h}} + n_{\text{a}} + n_{\text{c}} = 3, 5,$ and 101 under the conditions $n_{\text{a}} = 1$ and $n_{\text{c}} = n_{\text{h}}$. The equilibrium separation of the harmonic potential was set to $a = 2^{1/6} \sigma_{\text{Ar}}$, which is the minimum location for the Lennard-Jones potential of Ar used in Ref. [19] and $\sigma_{\text{Ar}} = 3.405 \text{ \AA}$. As mentioned in Sec. II A, the spring constant was $k = 1.3 \text{ J/m}^2$ for all particles, and particle mass values are as listed in Table I. For the a-particle mass m_{a} , 11 values in the range $0.1 \leq \chi_{\text{a}} \leq 5.0$ were examined in terms of the scaled a-particle mass $\chi_{\text{a}} \equiv m_{\text{a}}/m_{\text{c}}$. The thermostat temperatures were set to $T_{\text{h}} = 70 \text{ K}$ and $T_{\text{c}} = 30 \text{ K}$. These values were chosen to account for the fact that $T_{\text{h}} - T_{\text{c}}$ must be sufficiently large to limit statistical error, although lower temperature is desirable for numerical stability. The damping coefficient has the unit of angular frequency. We set $\eta_{\text{h}} = 8 \text{ rad/ps}$ (1.3 THz) for the hot thermostat and $\eta_{\text{c}} = 4 \text{ rad/ps}$ (0.64 THz) for the cold thermostat. In our 1D model, η_{h} and η_{c} are adjustable parameters that can affect physical quantities, unlike in the normal use of Langevin thermostats. The values of η_{h} and η_{c} described above were adjusted by trial and error to roughly reproduce the essential results of the reference system that the minimum ITR is reached at $\chi_{\text{a}} = 0.2\text{--}0.3$, as mentioned in Sec. II A. In addition, the value of η_{μ} must be sufficiently close to the vibrational frequencies of μ -particles. Otherwise,

an artificial thermal resistance may arise between the thermostat and reservoir particles, preventing proper temperature control. A further rationale from the NEGF theory for the selected values of η_{h} and η_{c} will be discussed in Sec. III D.

Initially, the chain particles were aligned at the equilibrium positions with zero velocity. After a 1 ns relaxation to ensure a nonequilibrium steady state under constant heat current, the production simulation was conducted for $\tau = 50 \text{ ns}$ using a simulation time step of 0.1 fs.

ITR R_{MD} was calculated by

$$R_{\text{MD}} = (T_{\text{h}} - T_{\text{c}})/J, \quad (30)$$

where $J = (e_{\text{h}} - e_{\text{c}})/(2\tau)$ is the average heat current, and $e_{\text{h}} > 0$ and $e_{\text{c}} < 0$ are the energy input from the hot and cold Langevin thermostats to the system, respectively, during the production run. We note that to be consistent with the NEGF theory, T_{h} and T_{c} in Eq. (30) must be the setting temperatures of the thermostats, whereas usual nonequilibrium MD simulations use the temperature difference at the interface obtained from extrapolating linear temperature profiles on both sides of the interface [16]. The VDOS was calculated from the Fourier transform of the VACF,

$$D_{\nu}(t) = \sum_{j \in \nu} m_j \langle \dot{x}_j(0) \dot{x}_j(t) \rangle, \quad (31)$$

where $\nu = \text{h, a, or c}$ denotes the particle species. The statistical error of any physical quantity was estimated as the standard error of mean over the five average values obtained from the five 10 ns blocks of the production simulation.

III. RESULTS AND DISCUSSION

A. Interfacial thermal resistance

Using MD simulation, ITR of the 1D chain was calculated as a function of the scaled a-particle mass $\chi_{\text{a}} = m_{\text{a}}/m_{\text{c}}$. The results for three different chain lengths were plotted in Fig. 2 in comparison to the theoretical curves by the NEGF method using the same parameters as those in the MD simulation. For the interested reader, examples of temperature profile along the chain are shown in the Supplemental Material (Fig. S1 [29]). The NEGF curves are in excellent agreement with the MD results, indicating that, in addition to the analytical solution, MD simulations with a combination of classical Langevin thermostats can also be employed to study the interfacial thermal transport described within the NEGF framework as long as the parameters including the damping coefficients and particle masses are carefully adjusted. In the reference system, the ITR- χ_{a} curve was downward convex and the minimum location $\chi_{\text{a},\text{min}}$ was found in the range $\chi_{\text{a},\text{min}} = 0.2\text{--}0.3$. The 1D model can reproduce this feature even in the case of the shortest possible chain, $n_{\text{tot}} = 3$, although it was difficult to reproduce the absolute values of ITR. It is therefore expected that the underlying mechanism of the ITR minimization in the 1D model is the same as that in the reference system. It is considered that the minimum location $\chi_{\text{a},\text{min}}$ is determined so that the characteristic (PMF) frequency in the a-particle system most effectively bridges those in the h- and c-reservoirs under given damping coefficients. Since the PMF frequency is described by the affinity (spring constant) and particle mass, the value of $\chi_{\text{a},\text{min}}$ in general is also affected

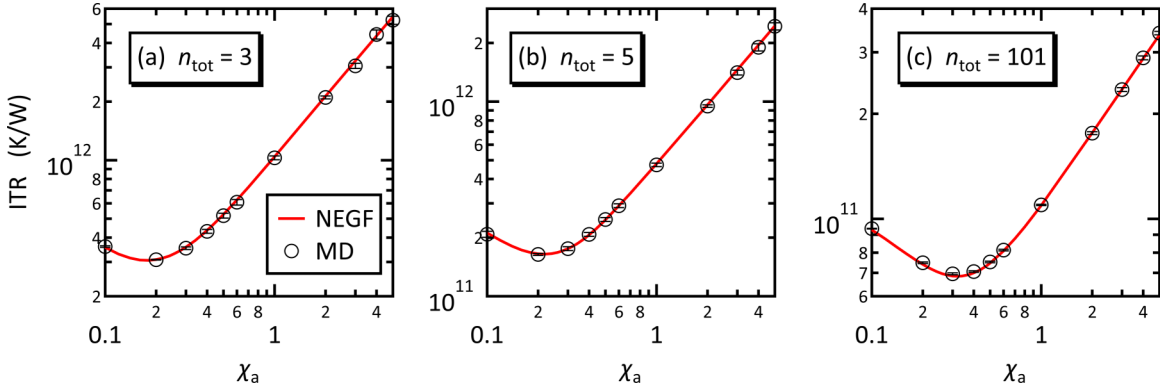


FIG. 2. Interfacial thermal resistance of the 1D chain model is plotted as a function of the scaled a-particle mass $\chi_a = m_a/m_c$. Parts (a), (b), and (c) show the results for the systems with different chain lengths $n_{\text{tot}} = 3, 5,$ and 101 , respectively. The red lines are the analytic solutions by the NEGF theory, while MD results are shown by the black circles with error bars.

by the affinity between the solid, adsorption layer, and bulk liquid. In the present study, however, the difference in affinity was renormalized into the difference in particle mass, i.e., the effect of affinity is implicitly included in that of particle mass. The optimal a-particle mass of $m_a = m_c \chi_{a,\text{min}} = 8\text{--}12$ u lies between $m_h = 1.381$ u and $m_c = 39.95$ u, which is consistent with the idea that the PMF frequency of a-particles bridges those of h- and c-particles.

A detailed chain length dependence of the minimum location is plotted in Fig. 3. For short chains, the minimum location slightly changes with n_{tot} , but it converges to $\chi_{a,\text{min}} = 0.32$ for $n_{\text{tot}} > 25$, or, equivalently, $n_\mu > 12$. This result implies that the mean free path of vibration modes in a reservoir is about 12 particles long. The mean free path is affected by the damping coefficient and the PMF frequency in Eq. (4) for the h- and c-reservoirs. The damping coefficient, which corresponds to the reciprocal of the mean free time, is negatively correlated with the mean free path. In contrast, the PMF frequency is positively correlated with the mean free path, as

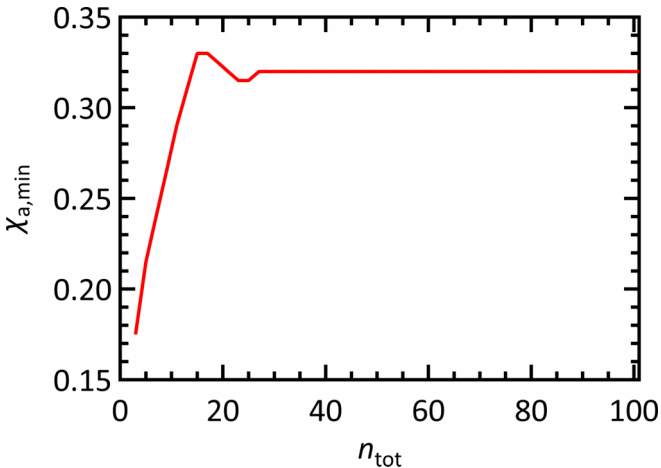


FIG. 3. Chain length dependence of the location of the ITR minimum calculated by the NEGF theory. The left axis is the scaled a-particle mass that gives the minimum ITR. The bottom axis is the chain length in terms of $n_{\text{tot}} = n_h + n_a + n_c$ under the conditions $n_a = 1$ and $n_h = n_c$.

is approximately explained by the fact that the speed of sound in a 1D harmonic chain is proportional to $(k/m)^{1/2}$ [24], where k and m are the spring constant and mass of the chain particle, respectively.

B. Vibrational density of states

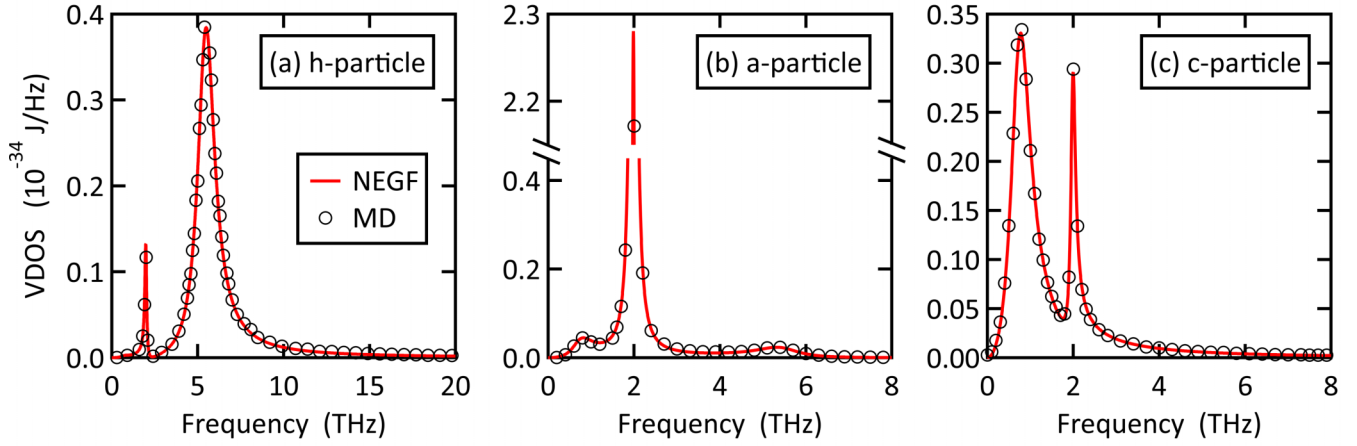
In Fig. 4, the vibrational density of states (VDOS) profiles for the h-, a-, and c-particles, D_h , D_a , and D_c , respectively, are shown in comparison with the MD results for $n_{\text{tot}} = 3$ with $\chi_a = 0.2$ and for $n_{\text{tot}} = 101$ with $\chi_a = 0.3$. [The two cases are the ones with the minimum ITR in Figs. 2(a) and 2(c).] The VDOS profiles of the reservoir particles for the $n_{\text{tot}} = 101$ case are normalized by the number of μ -particles as $D_\mu(\omega)/n_\mu$ so that all profiles in Fig. 4 are per single particle. The error bars of the MD results are not displayed for better visibility, but they are smaller than the circle markers. The NEGF curves are in excellent agreement with the MD results.

Figures 4(a)–4(c) are the VDOS profiles in the case of $n_{\text{tot}} = 3$ with $\chi_a = 0.2$, where each reservoir has only one particle. The VDOS of the a-particle in Fig. 4(b) is composed of a prominent peak at near the PMF frequency of the a-particle of 2.2 THz and secondary peaks at ~ 1.0 and ~ 5.36 THz due to the transmitted vibrations from the c- and h-reservoirs, respectively. Similarly, the VDOS profiles of the h-particle [Fig. 4(a)] and the c-particle [Fig. 4(c)] have a primary peak at its own PMF frequency, and a secondary peak coming from the a-particle vibration. As illustrated in Figs. 4(d) and 4(f), when the number of reservoir particles increases to $n_\mu = 50$, one a-particle peak and 50 μ -particle peaks in D_μ overlap each other to form a broad spectrum at around the PMF frequency. As shown in Fig. 4(e), a similar change occurs in D_a , although the a-particle peak remains relatively sharp.

The μ -particle peaks in D_μ [Eq. (25)] and D_a [Eq. (24)] originate from those in the reservoir Green's function \mathbf{g}_μ . By the inverse Fourier transform of Eq. (13), \mathbf{g}_μ in the time domain is proven to be

$$\mathbf{g}_\mu(t) = -\frac{2\pi}{\omega_\mu} e^{-\frac{\eta_\mu}{2}t} \sin(\omega_\mu t) \theta(t), \quad (32)$$

$$n_{\text{tot}} = 3, \chi_a = 0.2$$



$$n_{\text{tot}} = 101, \chi_a = 0.3$$

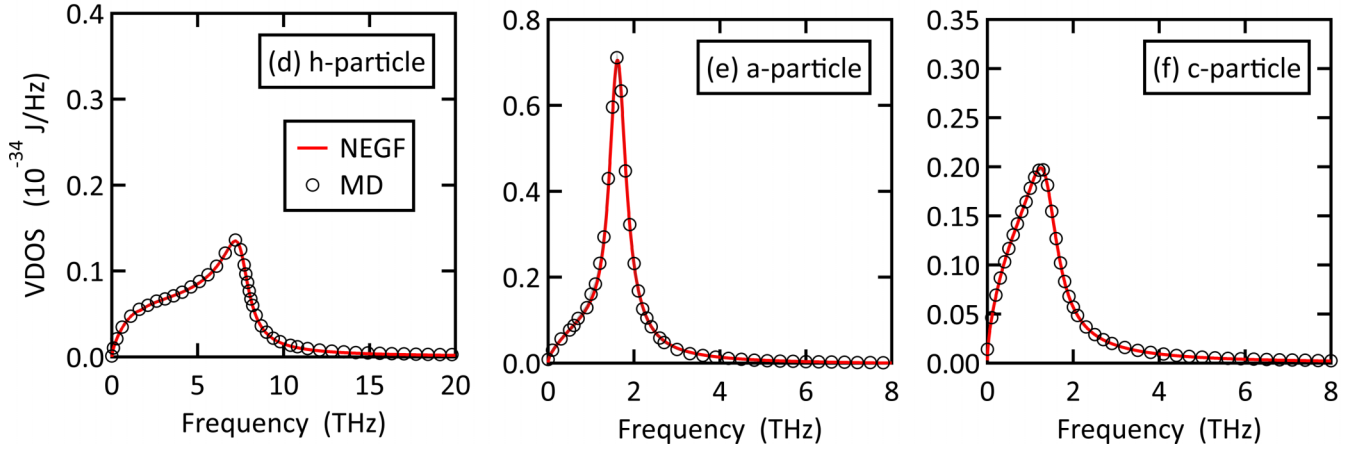


FIG. 4. VDOS profiles normalized by the number of particles. Parts (a), (b), and (c) are the results for the h-, a-, and c-particles, respectively, in the case of $n_{\text{tot}} = 3$ and $\chi_{\text{as}} = 0.2$, while (d), (e), and (f) are those for $n_{\text{tot}} = 101$ and $\chi_a = 0.3$. The red lines show the analytic solution by the NEGF theory, while the black circles show the MD results.

where $\theta(t)$ is the Heaviside step function, and

$$\omega_\mu = \sqrt{\mathbf{K}_\mu - \eta_\mu^2/4} \quad (33)$$

is an $n_\mu \times n_\mu$ matrix. The positions of μ -particle peaks are determined by the n_μ eigenvalues of ω_μ . As the effect of energy dissipation, the damping coefficient shifts these frequencies as in Eq. (33) and attenuates the vibration modes in time as $\exp(-\eta_\mu t/2)$. The latter results in the broadening of μ -particle peaks. Likewise, the a-particle peak comes from \mathbf{g}_a , where $\Gamma_h + \Gamma_c$ plays a similar role to η_μ .

C. Vibrational matching mechanism of the ITR minimization

Let us now consider how the ITR is minimized in terms of vibration-mode matching. For convenience, we examine the maximum of ITC in Eq. (29) instead of the minimum of ITR. In the present case of $n_a = 1$, Γ_μ , \mathbf{K}_a , Σ_μ , and \mathbf{g}_a are scalar quantities, and we will emphasize this by denoting them without boldface as Γ_μ , K_a , Σ_μ , and g_a , respectively. The transmission function α in Eq. (28) can be decomposed

into the two partial contributions α_{hc} and α_a :

$$\begin{aligned} \alpha(\omega) &= \frac{4\Gamma_h\Gamma_c}{(\Gamma_h + \Gamma_c)^2 + 4(\omega^2 - K_a - \text{Re}[\Sigma_h + \Sigma_c])^2} \\ &\equiv \alpha_{\text{hc}}(\omega)\alpha_a(\omega). \end{aligned} \quad (34)$$

The first partial transmission function is expressed as

$$\alpha_{\text{hc}}(\omega) = 4\Gamma_h\Gamma_c/(\Gamma_h + \Gamma_c)^2. \quad (35)$$

Directly evaluating $\Gamma_\mu = \mathbf{K}_{\mu a}^+ i[\mathbf{g}_\mu - \mathbf{g}_\mu^+] \mathbf{K}_{\mu a}$, one can find that $\Gamma_\mu \propto 1/m_a$, and therefore α_{hc} is independent of m_a . We also note that α_{hc} is a real-valued function satisfying $0 \leq \alpha_{\text{hc}} \leq 1$, and the maximum value 1 is reached when $\Gamma_h = \Gamma_c$. In addition, as Polanco *et al.* pointed out [28], if one interprets Γ_μ as a generalized acoustic impedance of the μ -reservoir, Eq. (35) is the transmission coefficient between the h- and c-reservoirs in the AMM model [10]. While α_{hc} thus describes the transmission between the two reservoirs, the m_a dependence of α is explained by the second partial transmission

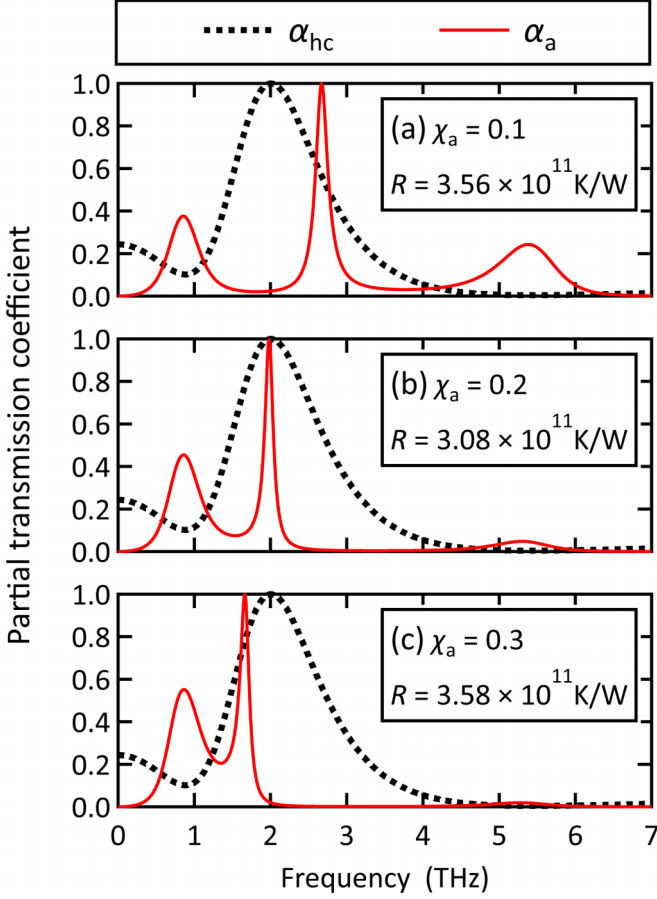


FIG. 5. Overlap between the partial transmission functions α_{hc} (black dotted lines) and α_a (red solid lines) for the case of $n_{\text{tot}} = 3$. Parts (a), (b), and (c) compare the curves for different values of the scaled a-particle mass χ_a . The value of the interfacial thermal resistance for each case is also included as R .

function α_a :

$$\alpha_a(\omega) = \frac{1}{1 + 4[\omega^2 - K_a - \text{Re}[\Sigma_h + \Sigma_c]]^2 / (\Gamma_h + \Gamma_c)^2}. \quad (36)$$

This function also satisfies $0 \leq \alpha_a \leq 1$, and the maximum value 1 is achieved at $\omega^2 = K_a + \text{Re}[\Sigma_h + \Sigma_c]$ or $\Gamma_\mu \rightarrow \infty$. With this decomposition, ITC is expressed by an inner product of α_{hc} and α_a as

$$G = \frac{k_B}{2\pi} \int_0^\infty \alpha_{hc}(\omega) \alpha_a(\omega) d\omega. \quad (37)$$

Since both α_{hc} and α_a are normalized as $0 \leq \alpha_{hc}, \alpha_a \leq 1$, the more similar α_{hc} and α_a are, the higher the ITC. In this sense, Eq. (37) describes ITC as the overlap of α_{hc} and α_a .

In Fig. 5, this situation is illustrated for the case of the shortest chain $n_{\text{tot}} = 3$. Just like the VDOS curves, both α_{hc} and α_a are characterized by multiple peaks. Comparing Figs. 5(a)–5(c), one can see that as χ_a increases from 0.1 to 0.3, the position of the middle peak in α_a moves to the low-frequency side, and at $\chi_a = 0.2$, this peak best overlaps with the peak of α_{hc} . Correspondingly, ITR in Fig. 2(a) is minimized at this value of χ_a . As mentioned above, the prominent peak of α_{hc} at ~ 2 THz is determined by the condition

$\Gamma_h = \Gamma_c$. As for α_a , the three peaks are originated from the c-, a-, and h-particles, in the order from the low-frequency side. The h- and c-particle peaks occur by the condition $\Gamma_\mu \rightarrow \infty$, reflecting the peaks in \mathbf{g}_μ , whose positions are given by Eq. (33) and are independent of m_a . These reservoir peaks in α_a do not significantly contribute to the total transmission function α because $\alpha_{hc} \rightarrow 0$ as $\Gamma_\mu \rightarrow \infty$. Consequently, of the three peaks of α_a , the a-particle peak, whose position is given by the condition $\omega^2 = K_a + \text{Re}[\Sigma_h + \Sigma_c]$, makes a dominant contribution to α . This vibrational matching principle is essentially the same for longer chains, although the detailed shapes of the peaks in α_{hc} and α_a become more complicated (Fig. S2 [29]). It might appear from Fig. 5 that ITR is minimized when α_a and α_{hc} have peaks at the same position, but this is not an essential condition. [In Fig. S2(b) [29], the ITR minimum occurs without the matching of peak positions.] The ITR minimum is always determined by the maximum of Eq. (37). It is expected, however, that the ITR minimum is often accompanied by such a coincidence of peak positions, since an inner product of two peak-shaped functions is usually maximized when their peak positions are the same. The overlap between α_{hc} and α_a in the form of Eq. (37) thus provides a quantitative model of the vibration-mode matching in the 1D chain. However, methods for estimating α_{hc} and α_a for real interfaces must be considered in the future.

It is beneficial to see the relation between the transmission function and VDOS. To this aim, it is convenient to express the transmission function $\alpha = \Gamma_h \delta_a^* \Gamma_c g_a$ in a resistance form as

$$\frac{1}{\alpha(\omega)} = \frac{1}{A(\omega)\Gamma_h(\omega)} + \frac{1}{A(\omega)\Gamma_c(\omega)}, \quad (38)$$

where $A(\omega) = g_a(\omega)[\Gamma_h(\omega) + \Gamma_c(\omega)]g_a^*(\omega)$ [see also Eq. (A4) in the Appendix]. From Eq. (24), expressing $T_h = T + \Delta T$ and $T_c = T - \Delta T$ with a small temperature difference ΔT , we find the following relation between $A(\omega)$ and the a-particle VDOS:

$$A(\omega) = \frac{2\pi D_a(\omega)}{k_B T \omega} + O\left(\frac{\Delta T}{T}\right). \quad (39)$$

On the other hand, Γ_μ is related to the reservoir VDOS at the uncoupled state, \mathbf{D}_μ^0 , as

$$\Gamma_\mu(\omega) = \frac{2\pi}{\omega k_B T_\mu} \mathbf{K}_{\mu a}^+ \mathbf{D}_\mu^0(\omega) \mathbf{K}_{\mu a}, \quad (40)$$

as shown in Eq. (A3) in the Appendix. Equations (39) and (40) are used to approximate $A\Gamma_\mu$ in Eq. (38) as

$$A(\omega)\Gamma_\mu(\omega) = \left(\frac{2\pi}{k_B T \omega}\right)^2 \mathbf{K}_{\mu a}^+ \mathbf{D}_\mu^0(\omega) \mathbf{K}_{\mu a} D_a(\omega) + O\left(\frac{\Delta T}{T}\right). \quad (41)$$

From this relation together with Eq. (38), one can see that in addition to the VDOS overlap between \mathbf{D}_μ^0 and D_a , the strength of interfacial coupling, $\mathbf{K}_{\mu a}$, also makes a positive contribution to the transmission function. Equations (38) and (41) would provide a useful starting point for theoretical considerations of various kinds of correlations between thermal transport and affinity at solid-liquid interfaces, which have been found in many studies [3–7].

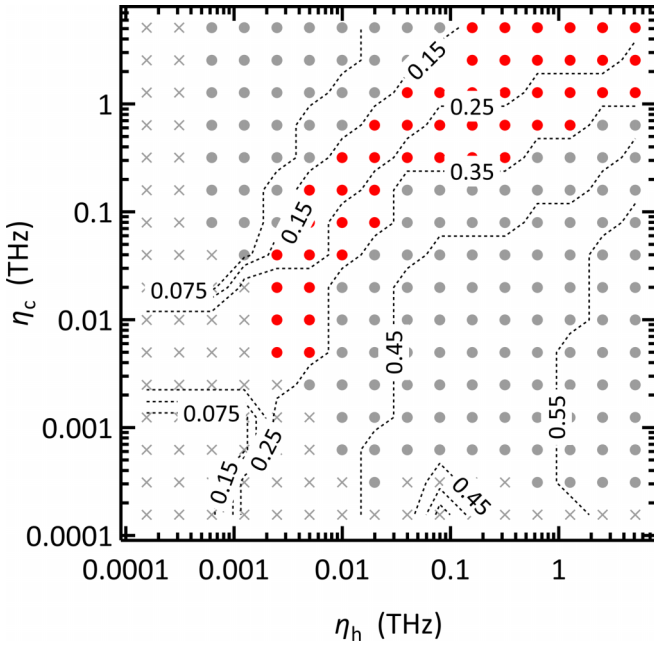


FIG. 6. Contour of the minimum location of ITR- χ_a curve, $\chi_{a,\min}$, for the chain with $n_{\text{tot}} = 101$. A calculation point is denoted by a filled circle or a cross depending on whether the ITR- χ_a curve is downward convex with a single minimum or not, respectively. The calculation points that well reproduce the results of the reference system with $\chi_{a,\min} = 0.2\text{--}0.3$ are emphasized by red.

D. Role of the damping coefficient

One-dimensional harmonic chains similar to the present model have been used to model ballistic phonon transport at the junction of solid nanomaterials in the NEGF [28,30,31] and other [32,33] formalisms. An important difference between the present model and the existing ones exists in the magnitude of the damping coefficients. In the existing models, η_μ is a positive infinitesimal value, as is generally assumed in the NEGF theory [12,20,34].

In contrast, the results of the present analysis indicate that much larger values of η_μ are necessary for the 1D chain to model solid-liquid interfaces, where diffusive thermal transport also makes a significant contribution. Figure 6 illustrates the minimum location of the ITR- χ_a curve as a function of η_h and η_c in the case of $n_{\text{tot}} = 101$. In addition to the pair of η_h and η_c adopted in the previous sections, many other pairs indicated by the filled red circles can yield the ITR- χ_a curve that has a single minimum in the range $\chi_a = 0.2\text{--}0.3$. However, no such pair is found if the damping coefficients are as small as $\eta_h < 0.002$ THz or $\eta_c < 0.004$ THz. In particular, for the η_h and η_c pairs denoted by the cross markers, the ITR- χ_a curve exhibited oscillations and multiple minima. In this example, the damping coefficient must be of a similar order of magnitude to the PMF frequencies of the reservoir particles. It is worth noting that under this condition, some eigenvalues of ω_μ in Eq. (33) can be imaginary, corresponding to overdamped modes. In the case of the 101-particle chain with $\eta_h = 1.3$ THz and $\eta_c = 0.64$ THz, for example, the matrix diagonalization revealed that out of 50 eigenvalues for each of ω_h and ω_c , two and seven were imaginary,

respectively. Recently, it was reported that such imaginary frequencies due to overdamping are essential to explain the low-frequency behavior of VDOS in liquids [35]. Whether or not ω_μ has imaginary eigenvalues, the large damping coefficients seem necessary to represent the rapid attenuation of vibration modes at solid-liquid interfaces where diffusive thermal transport makes a significant contribution. This idea does not always contradict the existing models, which use infinitesimal damping coefficients to describe interfacial thermal transport in solids governed by ballistic phonons.

IV. CONCLUSION

In the present study, interfacial thermal transport at interfaces between solids and surfactant solutions was considered using a 1D harmonic chain model. The analytical expression for the ITR of the 1D chain was derived using the NEGF theory, which led to an explicit expression of vibration-mode matching [Eq. (37)]. The 1D chain is expected to model solid-liquid interfaces in general because the a-particle does not necessarily have to be a surfactant layer. Although a harmonic chain cannot represent the fluidity of liquids, this is not an essential issue. Because the purpose of the 1D chain is to model the transmission of characteristic vibrations across a solid-liquid interface, it is sufficient if a harmonic chain can represent the characteristic frequency in the liquid region. The PMF frequency may qualify as such a characteristic frequency in liquids.

In our model, the equation of motion for the chain particles was described by a fully classical Langevin equation, which not only allowed a precise comparison with the classical MD simulation, but also facilitated the physical interpretation of mathematical expressions. In particular, the damping coefficient η_μ in our interpretation plays an important role in modeling the energy dissipation associated with phonon scattering. In the case of a liquidlike system, a large value of η_μ is required to represent the rapid damping of vibrational modes. In contrast, η_μ may be infinitesimal, as in the conventional NEGF theory, in the case of solidlike interfaces characterized by phonons with long lifetimes. Even though this concept is only based on a simple one-dimensional model, it may provide a clue for extending the phonon transmission picture of thermal transport at hard interfaces to softer interfaces.

ACKNOWLEDGMENTS

This work was supported by JST CREST Grant No. JPMJCR1712, Japan. Computational simulations were performed on the supercomputer system “AFI-NITY” at the Advanced Fluid Information Research Center, Institute of Fluid Science, Tohoku University.

APPENDIX: SUPPLEMENT TO THE DERIVATION OF THE NEGF EXPRESSIONS

In this appendix, we supplement the derivation of the NEGF expressions in Sec. II B. We omit the argument ω of frequency-dependent variables when it is obvious. In addition, if a term includes two frequencies like $X^+(\omega')Y(\omega)$, variables

with and without superscript + are considered to depend on ω' and ω , respectively, unless otherwise indicated.

Let us first prepare some identities. From Eq. (13), $i[(\mathbf{g}_\mu^+)^{-1} - \mathbf{g}_\mu^{-1}] = 2\omega\boldsymbol{\eta}_\mu$ holds, since both \mathbf{K}_μ and $\boldsymbol{\eta}_\mu$ are real symmetric matrices. Multiplying both sides of this equation by \mathbf{g}_μ from the left and by \mathbf{g}_μ^+ from the right, or vice versa, one can show that

$$i[\mathbf{g}_\mu - \mathbf{g}_\mu^+] = 2\omega\mathbf{g}_\mu\boldsymbol{\eta}_\mu\mathbf{g}_\mu^+ = 2\omega\mathbf{g}_\mu^+\boldsymbol{\eta}_\mu\mathbf{g}_\mu. \quad (\text{A1})$$

This quantity is called the spectral function [21], which describes the energy spectrum of μ -particles. Using Eqs. (19), (20), and (A1), we have another expression for Γ_μ :

$$\Gamma_\mu = 2\omega\mathbf{K}_{\mu a}^+\mathbf{g}_\mu\boldsymbol{\eta}_\mu\mathbf{g}_\mu^+\mathbf{K}_{\mu a}, \quad (\text{A2})$$

or, in terms of the reservoir VDOS at the uncoupled state, \mathbf{D}_μ^0 , in Eq. (23), one can write

$$\Gamma_\mu = \frac{2\pi}{\omega k_B T_\mu} \mathbf{K}_{\mu a}^+ \mathbf{D}_\mu^0 \mathbf{K}_{\mu a}. \quad (\text{A3})$$

Just as we did for \mathbf{g}_μ in Eq. (A1), the spectral function for a-particles can be expressed as

$$i[\mathbf{g}_a - \mathbf{g}_a^+] = \mathbf{g}_a(\Gamma_h + \Gamma_c)\mathbf{g}_a^+ = \mathbf{g}_a^+(\Gamma_h + \Gamma_c)\mathbf{g}_a, \quad (\text{A4})$$

using Eqs. (18) and (20). Multiplying Γ_h on both sides of the last equality in Eq. (A4) and taking the trace, we can find that the Γ_h and Γ_c in the transmission function Eq. (28) are interchangeable,

$$\text{Tr}[\Gamma_h \mathbf{g}_a \Gamma_c \mathbf{g}_a^+] = \text{Tr}[\Gamma_c \mathbf{g}_a \Gamma_h \mathbf{g}_a^+]. \quad (\text{A5})$$

Next, we derive some correlations among displacement vectors. From \mathbf{u}_μ^0 in Eq. (15) and the fluctuation-dissipation relation Eq. (21), we have

$$\langle \mathbf{u}_\mu^0(\omega) \mathbf{u}_{\mu'}^{0+}(\omega') \rangle = \mathbf{g}_\mu \frac{\boldsymbol{\eta}_\mu k_B T_\mu}{\pi} \mathbf{g}_\mu^+ \delta(\omega - \omega') \delta_{\mu\mu'}. \quad (\text{A6})$$

Combining Eqs. (A2) and (A6) gives

$$\mathbf{K}_{\mu a} \langle \mathbf{u}_\mu^0(\omega) \mathbf{u}_{\mu'}^{0+}(\omega') \rangle \mathbf{K}_{\mu' a}^+ = \frac{k_B T_\mu}{2\pi\omega} \Gamma_\mu \delta(\omega - \omega') \delta_{\mu\mu'}. \quad (\text{A7})$$

This equation can be used to calculate the correlations relevant to \mathbf{u}_a in Eq. (17):

$$\begin{aligned} \langle \mathbf{u}_a(\omega) \mathbf{u}_a^+(\omega') \rangle &= \sum_{\mu=h,c} \sum_{\mu'=h,c} \mathbf{g}_a(\omega) \mathbf{K}_{\mu a}^+ \langle \mathbf{u}_\mu^0(\omega) \mathbf{u}_{\mu'}^{0+}(\omega') \rangle \\ &\quad \times \mathbf{K}_{\mu' a} \mathbf{g}_a^+(\omega') \\ &= \sum_{\mu=h,c} \frac{k_B T_\mu}{2\pi\omega} \mathbf{g}_a \Gamma_\mu \mathbf{g}_a^+ \delta(\omega - \omega') \end{aligned} \quad (\text{A8})$$

and

$$\langle \mathbf{u}_a(\omega) \mathbf{u}_\mu^{0+}(\omega') \rangle \mathbf{K}_{\mu a} = \frac{k_B T_\mu}{2\pi\omega} \mathbf{g}_a \Gamma_\mu \delta(\omega - \omega'). \quad (\text{A9})$$

The VDOS expressions Eqs. (24) and (25) can be obtained using Eqs. (A8) and (A9), as we did in Eq. (22) for the uncoupled case.

As shown in Eq. (26), the heat current from the μ -reservoir to the a-particle system is

$$J_{\mu a}(t) = \iint J_{\mu a}(\omega, \omega') e^{-i(\omega-\omega')t} d\omega' d\omega, \quad (\text{A10})$$

where the spectral heat current is given by

$$\begin{aligned} J_{\mu a}(\omega, \omega') &= \frac{i\omega'}{2} \langle \mathbf{u}_\mu^+ \mathbf{K}_{\mu a} \mathbf{u}_a - \mathbf{u}_a^+ \mathbf{K}_{\mu a}^+ \mathbf{u}_\mu \rangle \\ &= \frac{i\omega'}{2} \text{Tr} \langle \mathbf{u}_a \mathbf{u}_\mu^+ \mathbf{K}_{\mu a} - \mathbf{K}_{\mu a}^+ \mathbf{u}_\mu \mathbf{u}_a^+ \rangle. \end{aligned} \quad (\text{A11})$$

If we apply $\mathbf{u}_\mu = \mathbf{u}_\mu^0 + \mathbf{g}_\mu \mathbf{K}_{\mu a} \mathbf{u}_a$ [Eq. (16)], $J_{\mu a}$ is divided into two parts:

$$J_{\mu a}(\omega, \omega') = J_1(\omega, \omega') + J_2(\omega, \omega'). \quad (\text{A12})$$

The first term J_1 comes from the \mathbf{u}_μ^0 part of \mathbf{u}_μ :

$$\begin{aligned} J_1(\omega, \omega') &= \frac{i\omega'}{2} \text{Tr} [(\mathbf{u}_a \mathbf{u}_\mu^{0+}) \mathbf{K}_{\mu a} - \mathbf{K}_{\mu a}^+ (\mathbf{u}_\mu^0 \mathbf{u}_a^+)] \\ &= \frac{k_B T_\mu}{4\pi\omega} i \text{Tr} [\mathbf{g}_a \Gamma_\mu - \Gamma_\mu^+ \mathbf{g}_a^+] \delta(\omega - \omega') \\ &= \frac{k_B T_\mu}{4\pi\omega} \text{Tr} [\mathbf{g}_a (\Gamma_h + \Gamma_c) \mathbf{g}_a^+ \Gamma_\mu] \delta(\omega - \omega'), \end{aligned} \quad (\text{A13})$$

where Eq. (A9) was used to obtain the second line, and then $\text{Tr}[\Gamma_\mu^+ \mathbf{g}_a^+] = \text{Tr}[\mathbf{g}_a^+ \Gamma_\mu^+]$, $\Gamma_\mu^+ = \Gamma_\mu$, and Eq. (A4) were used to yield the final result. The second term J_2 in Eq. (A12) is due to the $\mathbf{g}_\mu \mathbf{K}_{\mu a} \mathbf{u}_a$ part of \mathbf{u}_μ . Considering $\boldsymbol{\Sigma}_\mu(\omega) = \mathbf{K}_{\mu a}^+ \mathbf{g}_\mu(\omega) \mathbf{K}_{\mu a}$ [Eq. (19)], this term is written as

$$\begin{aligned} J_2(\omega, \omega') &= \frac{i\omega'}{2} \text{Tr} [(\mathbf{u}_a \mathbf{u}_a^+) \boldsymbol{\Sigma}_\mu^+ - \boldsymbol{\Sigma}_\mu (\mathbf{u}_a \mathbf{u}_a^+)] \\ &= \sum_{v=h,c} \frac{k_B T_v}{4\pi} i \text{Tr} [\mathbf{g}_a \Gamma_v \mathbf{g}_a^+ \boldsymbol{\Sigma}_\mu^+ - \boldsymbol{\Sigma}_\mu \mathbf{g}_a \Gamma_v^+ \mathbf{g}_a^+] \\ &\quad \times \delta(\omega - \omega') \\ &= - \sum_{v=h,c} \frac{k_B T_v}{4\pi} \text{Tr} [\mathbf{g}_a \Gamma_v \mathbf{g}_a^+ \Gamma_\mu] \delta(\omega - \omega'), \end{aligned} \quad (\text{A14})$$

where Eq. (A8) was used to obtain the second line, and then Eq. (A5) and $\Gamma_\mu = i[\boldsymbol{\Sigma}_\mu - \boldsymbol{\Sigma}_\mu^+]$ [Eq. (20)] were used to yield the final result. Expressing the spectral heat current $J_{\mu a}(\omega, \omega')$ by Eqs. (A13) and (A14) and inserting it into Eq. (A10), we have the final expression for the average heat current:

$$\begin{aligned} J_{\mu a}(t) &= \frac{k_B}{4\pi} (2T_\mu - T_h - T_c) \int_{-\infty}^{\infty} \alpha(\omega) d\omega \\ &= \frac{k_B}{2\pi} (2T_\mu - T_h - T_c) \int_0^{\infty} \alpha(\omega) d\omega. \end{aligned} \quad (\text{A15})$$

The last equality follows from the fact that $\alpha(-\omega) = \alpha(\omega)$ holds because $\Gamma_\mu(-\omega) = -\Gamma_\mu(\omega)$ and $\mathbf{g}_a(-\omega) = \mathbf{g}_a^+(\omega)$. Setting $\mu = h$ in Eq. (A15), one obtains the heat current from the h-reservoir to the a-particle system, J_{ha} , in Eq. (27), whereas $\mu = c$ gives the heat current from the c-reservoir to the a-particle system, J_{ca} . Comparing these two, one finds $J_{ha} = -J_{ca}$ as expected.

- [1] R. Lenin, P. A. Joy, and C. Bera, *J. Mol. Liq.* **338**, 116929 (2021).
- [2] R. D. Pathumudy and K. N. Prabhu, *J. Mater. Sci. Mater. Electron.* **32**, 11339 (2021).
- [3] H. Harikrishna, W. A. Ducker, and S. T. Huxtable, *Appl. Phys. Lett.* **102**, 251606 (2013).
- [4] J. Park and D. G. Cahill, *J. Phys. Chem. C* **120**, 2814 (2016).
- [5] D. Huang, R. Ma, T. Zhang, and T. Luo, *ACS Appl. Mater. Interfaces* **10**, 28159 (2018).
- [6] S. Li, Y. Chen, J. Zhao, C. Wang, and N. Wei, *Nanoscale* **12**, 17870 (2020).
- [7] C. U. Gonzalez-Valle and B. Ramos-Alvarado, *ACS Appl. Nano Mater.* **4**, 3821 (2021).
- [8] A. Giri and P. E. Hopkins, *Adv. Funct. Mater.* **30**, 1903857 (2020).
- [9] J. S. Wang, J. Wang, and J. T. Lü, *Eur. Phys. J. B* **62**, 381 (2008).
- [10] E. T. Swartz and R. O. Pohl, *Rev. Mod. Phys.* **61**, 605 (1989).
- [11] K. Pietrak and T. S. Winiewski, *J. Power Technol.* **95**, 14 (2014).
- [12] J. S. Wang, J. Wang, and N. Zeng, *Phys. Rev. B* **74**, 033408 (2006).
- [13] T. Yamamoto and K. Watanabe, *Phys. Rev. Lett.* **96**, 255503 (2006).
- [14] P. K. Schelling, S. R. Phillpot, and P. Keblinski, *Appl. Phys. Lett.* **80**, 2484 (2002).
- [15] X. Wei and T. Luo, *J. Appl. Phys.* **126**, 015301 (2019).
- [16] Z. Liang and M. Hu, *J. Appl. Phys.* **123**, 191101 (2018).
- [17] Y. Guo, D. Surblys, Y. Kawagoe, H. Matsubara, X. Liu, and T. Ohara, *Int. J. Heat Mass Transf.* **135**, 115 (2019).
- [18] Y. Guo, D. Surblys, H. Matsubara, and T. Ohara, *J. Mol. Liq.* **335**, 116243 (2021).
- [19] H. Matsubara, D. Surblys, Y. Bao, and T. Ohara, *J. Mol. Liq.* **347**, 118363 (2022).
- [20] W. Zhang, T. S. Fisher, and N. Mingo, *Numer. Heat Transf. Part B Fundam.* **51**, 333 (2007).
- [21] S. Datta, *Quantum Transport: Atom to Transistor*, 2nd ed. (Cambridge University Press, New York, 2005).
- [22] A. Dhar and D. Roy, *J. Stat. Phys.* **125**, 801 (2006).
- [23] A. Dhar and R. Dandekar, *Phys. A Stat. Mech. Its Appl.* **418**, 49 (2015).
- [24] M. T. Dove, *Introduction to Lattice Dynamics* (Cambridge University Press, New York, 1993).
- [25] T. Ohara, *J. Chem. Phys.* **111**, 9667 (1999).
- [26] S. Plimpton, *J. Comput. Phys.* **117**, 1 (1995).
- [27] A. P. Thompson, H. M. Aktulga, R. Berger, D. S. Bolintineanu, W. M. Brown, P. S. Crozier, P. J. in 't Veld, A. Kohlmeyer, S. G. Moore, T. D. Nguyen, R. Shan, M. J. Stevens, J. Tranchida, C. Trott, and S. J. Plimpton, *Comput. Phys. Commun.* **271**, 108171 (2022).
- [28] C. A. Polanco, C. B. Saltonstall, P. M. Norris, P. E. Hopkins, and A. W. Ghosh, *Nanoscale Microscale Thermophys. Eng.* **17**, 263 (2013).
- [29] See Supplemental Material at <http://link.aps.org/supplemental/10.1103/PhysRevE.107.024103> for examples of temperature profile and the overlap between the partial transmission coefficients for $n_{\text{tot}} = 5$ and 101.
- [30] P. E. Hopkins, P. M. Norris, M. S. Tsegaye, and A. W. Ghosh, *J. Appl. Phys.* **106**, 063503 (2009).
- [31] C. B. Saltonstall, C. A. Polanco, J. C. Duda, A. W. Ghosh, P. M. Norris, and P. E. Hopkins, *J. Appl. Phys.* **113**, 013516 (2013).
- [32] L. Zhang, P. Keblinski, J. S. Wang, and B. Li, *Phys. Rev. B* **83**, 064303 (2011).
- [33] B. Chen and L. Zhang, *J. Phys.: Condens. Matter* **27**, 125401 (2015).
- [34] C. A. Polanco, *Nanoscale Microscale Thermophys. Eng.* **25**, 1 (2021).
- [35] A. Zaccone and M. Baggioli, *Proc. Natl. Acad. Sci. (U.S.A.)* **118**, e2022303118 (2021).